Lawrence Berkeley National Laboratory

Title

Calcite Twinning in Mollusk Shells and Carrara Marble

Permalink

https://escholarship.org/uc/item/91d183dg

Authors

Alvarez, Cristina Castillo
Grimsich, John L
Schmidt, Connor A
et al.

Publication Date

DOI

Copyright Information

Nanoelectronics and Its New Materials –
A NEW ERA OF NANOSCIENCE

Nanoelectronics and Its New Materials –
A NEW ERA OF NANOSCIENCE

ZEISS
Seeing beyond

WILEY
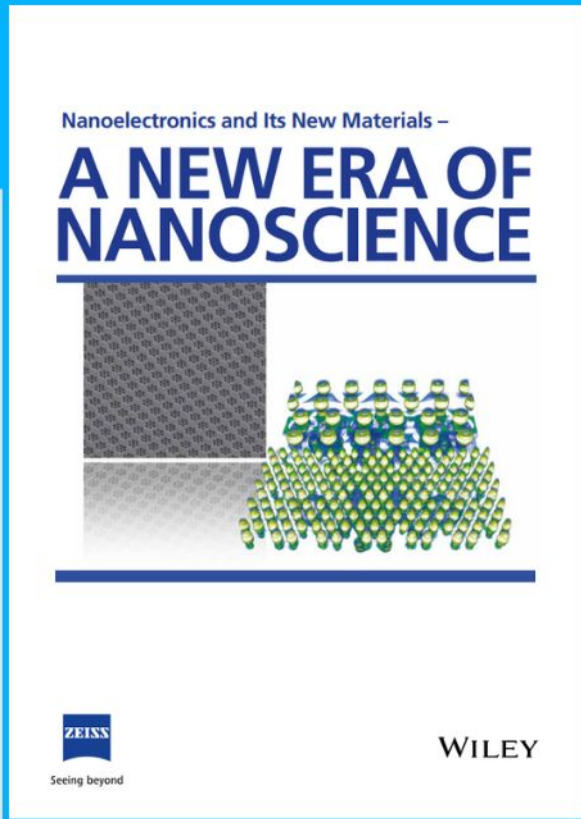
Discover the recent advances in electronics research and fundamental nanoscience.

Nanotechnology has become the driving force behind breakthroughs in engineering, materials science, physics, chemistry, and biological sciences. In this compendium, we delve into a wide range of novel applications that highlight recent advances in electronics research and fundamental nanoscience. From surface analysis and defect detection to tailored optical functionality and transparent nanowire electrodes, this eBook covers key topics that will revolutionize the future of electronics.

To get your hands on this valuable resource and unleash the power of nanotechnology, simply download the eBook now. Stay ahead of the curve and embrace the future of electronics with nanoscience as your guide.

ZEISS
Seeing beyond

WILEY

Calcite Twinning in Mollusk Shells and Carrara Marble

*Cristina Castillo Alvarez, John L. Grimsich, Connor A. Schmidt, Harrison Lisabeth, Anne Voigtländer, and Pupa U. P. A. Gilbert**

Mollusk shells protect the animals that form and inhabit them. They are composites of minerals and organics, with diverse mesostructures, including nacre, prismatic calcite, crossed-lamellar aragonite, and foliated calcite. Twins, that is, crystals mirror symmetric with respect to their coherent interface, occurring as formation or deformation twins, are observed in all mollusk shell mesostructures but never within calcite prisms. Here, nanotwins and microwins within single calcite prisms are observed in different shells. Using Polarization-dependent Imaging Contrast (PIC) mapping with 20–60 nm resolution, twins are observed to be 0.2–3 µm thick layers of differently oriented and colored crystals with respect to the main prism crystal. Multiple twins are interspersed with the prism crystal, parallel to one another, and similarly oriented. When comparing images of calcite prisms and twins obtained by PIC mapping and by Electron Back-Scattered Diffraction (EBSD), the images correspond precisely. All twins are e-twin types, with 127° angular distance between c-axes. E-twins are the most common deformation twins in geologic calcite, as also observed here in Carrara marble. Location of all twins near the outer surface of all shells and e-twin type both suggest that twins within calcite prisms in mollusk shells result from deformation twinning.

1. Introduction

Two crystals are twinned when they form along preferred planes, do not break bonds, and are tightly bonded to one another. The crystal lattices of both twins are mirror symmetric with respect to the twin plane. The twin plane is defined by atomic positions that are part of and coherent with the crystal lattices of both twins. In short, therefore: "the lattices of two twin crystals are mirror symmetric with respect to their coherent interface". W. Lawrence Bragg observed crystal twinning in aragonite ($CaCO_3$) and calcite almost 100 years ago, in 1924.[1]

Two adjacent twin crystals have a fixed relationship, termed twinning law, characteristic of each mineral structure. For calcite, four such symmetry operations are possible, described by Richards as "four and only four" calcite twinning laws.[2] These are summarized in **Table 1**. Remarkably, Pokroy et al. found a fifth twin in calcite crystals grown synthetically in the presence of a protein extracted from the mollusk shell *Pinna nobilis*.[3]

There are two kinds of twinning mechanisms, occurring during or after crystal growth, termed formation and deformation twinning, respectively.[4–8] Deformation twinning in calcite was observed extensively in rocks[6,9] and fossil shells,[10] but it was not observed in modern shells.

2. Twinning in Other Biominerals

In biominerals, formation twinning was observed extensively. In calcite brachiopod shells, formation twinning occurs, where

C. Castillo Alvarez, P. U. P. A. Gilbert
Chemical Sciences Division
Lawrence Berkeley National Laboratory
Berkeley, CA 94720, USA
E-mail: pupa@physics.wisc.edu

J. L. Grimsich
Department of Earth and Planetary Sciences
University of California Berkeley
Berkeley, CA 94720, USA

C. A. Schmidt, P. U. P. A. Gilbert
Department of Physics
University of Wisconsin
Madison, WI 53706, USA

H. Lisabeth, A. Voigtländer
Energy Geosciences Division
Lawrence Berkeley National Laboratory
Berkeley, CA 94720, USA

P. U. P. A. Gilbert
Departments of Chemistry, Materials Science and Engineering, Geoscience
University of Wisconsin
Madison, WI 53706, USA

**ADVANCED
SCIENCE NEWS**

www.advancedsciencenews.com

**ADVANCED
FUNCTIONAL
MATERIALS**

www.afm-journal.de

Table 1. Twin planes possible in calcite are crystal lattice planes (001), (012), (104), or (018). Twins mirror symmetric with respect to each of these planes are termed c-, f-, r-, and e- twins. The angle δ between crystallographic c-axes of calcite twin crystal and its host crystal.[2, 11] The angle γ is also the angular distance between c-axes, but it is different from δ because in PIC mapping the convention is to choose the smallest angle c-axes form in 3D space, thus, when δ is >90°, then $\gamma = 180° - \delta$.

Calcite twin type	Angle δ between c-axes	Angle γ in PIC mapping
c-twin (001)	180°	0°
f-twin (012)	54°	54°
r-twin (104)	91°	89°
e-twin (018)	127°	53°

adjacent twin crystals are as large as the entire lamellae in semi-nacre or foliated structures.[12] In foraminifera shells too, calcite formation twinning is observed, and it is templated by an organic sheet.[13] For reasons not well understood, in echinoderm calcite biominerals twinning is not observed.[14]

2.1. Twinning in Mollusk Shells

Several structures exist in mollusk shells, all different from one another in morphology, size, and shape, and orientation of calcite or aragonite crystals, all collectively termed "mesostructures"[15] described in detail by Taylor.[16] These mesostructures include aragonite nacre (e.g., inside abalone shells and pearl oysters),[17] crossed-lamellar aragonite structure (e.g., in conch shells),[18] foliated calcite also known as lamellar microstructure (e.g., in the windowpane oyster shell *Placuna placenta*, all edible oysters and scallops, and saddle shells),[7,19,20] and prismatic calcite (on the outer side of bivalve and gastropod shells, including the pteriidae *Pinctada* pearl oysters, the pinnidae *Pinna* and *Atrina*, and gastropods such as snails and abalone shells). Twinning was observed in most of these structures, but never within individual prisms of the calcite prismatic shell layer.

In *Pinna nobilis* shells, inter-prism macroscopic twin boundaries were observed between calcite prisms in the prismatic layer, where each prism is single crystalline and ≈10 μm wide.[21] In a similar shell, *Atrina rigida*, calcite prisms were observed to be harder than geologic calcite due to hindered dislocation motion, but this hardening was not associated with twinning, and twins were not observed in *Atrina rigida*, only in geologic calcite, in that work.[22]

In *Placuna placenta* shells, a toughening mechanism due to twinning was elegantly demonstrated at the nanoscale by Li and Ortiz, after artificial, nanoindentation-induced, deformation, nanotwinning of calcite in the foliated lamellar microstructure.[7] Li and Ortiz demonstrated that nanotwins make the shell more resistant to penetration of the indenter, and they keep the deformation localized resulting in approximately an order of magnitude greater energy dissipation in the shell than in geologic calcite.

In nacre, the inner lining of many gastropod, bivalve, and cephalopod shells, each aragonite tablet is multiply twinned.[23,24]

In the conch mollusk shell of *Strombus gigas* Shin et al. showed that naturally occurring aragonite nanotwins contribute significantly to the toughness of the crossed-lamellar structure of conch shells.[25] The crossed-lamellar is a well-known mollusk shell mesostructure, distinct from all others: nacre, prismatic, etc. In the crossed-lamellar structure there are three orders of lamellae, from 60 μm to 60 nm in size, with parallel aragonite needles, stacked so that the crystal orientations alternate by 90° at the 1st order. Zooming into this structure, there are more hierarchical levels with alternating orientations also for the 2nd and 3rd order lamellae.[18] Nanotwins add a 4th hierarchical level, and demonstrate that nanoscale twinning toughens the material by stopping crack propagation at twin interfaces, where cracks are deflected.[25] Crack deflection is a key toughening mechanism, well-established at multiple scales.[26,27]

Biominerals often achieve greater toughness than monolithic minerals.[11,18,28,29] Twinning significantly modifies the mechanical properties of biogenic minerals.[11] Twinning boundaries provide crack impeding and deflection in the biomineral building blocks.[11] Twinned crystals, therefore, have been interpreted as conferring mollusk shells mechanical improvements compared to untwinned crystals.[11]

Twinning has not been reported within individual prisms of the calcite prismatic layer of any mollusk shells. Do calcite twins exist naturally within mollusk shell calcite prisms? If so, are they formation or deformation twins? To answer these questions, we set out to explore the existence of twins in the calcite prismatic layer of various mollusk shells, using methods that provide simultaneously nano- or micro-scale resolution necessary to detect twins if they exist, surface sensitivity to analyze one crystal at a time in each image pixel, and measure the precise angles formed by twins with the calcite prism crystal.

3. Experimental Section

Pinctada margaritifera (*Pm*) dry shells were collected by one of the authors (PG) in 2004 from the Ferme Perlière Paul Gauguin, Rangiroa, French Polynesia. Sample Pm2-5 was analyzed during the April 2021 beamtime, here, area 3 from this sample in **Figure 1** was presented.

Sample Pm2-M3 was analyzed during the April 2022 beamtime, here, area 1 from this sample in Figure 1B was presented.

Sample Pm25-5 was analyzed during the June 2022 beamtime, here, area 1 from this sample in Figure 1C was presented. **Figure 2** shows two shells at once, Pm2-5 and Pm2-M3.

Calcite prisms in *Pm* had width 34 ± 10 μm (Avg ± St Dev, $n = 19$).

Haliotis rufescens (*Hr*) live animals and their shells were purchased in 2013 from the Monterey Abalone Company, Monterey, CA, USA. Sample Hr1-4 was analyzed during the June 2022 beamtime, here, area 1 from this sample in Figure 4 was presented.

Calcite prisms in *Hr* has width 25 ± 8 μm (Avg ± St Dev, $n = 18$).

Atrina rigida (*Ar*) live animals and their bivalve shells were purchased in 2014 from Gulf Specimen Marine Laboratory, Panacea, FL, USA. Sample Ar7-2 was analyzed during the June 2022 beamtime, here, areas 1 and 2 from this sample in Figure 5 were presented.

**ADVANCED
SCIENCE NEWS**

www.advancedsciencenews.com

**ADVANCED
FUNCTIONAL
MATERIALS**

www.afm-journal.de

Calcite prisms in *Ar* had width 21 ± 9 μm (Avg ± St Dev, *n* = 24).

Carrara marble (Cm) samples were collected by one of the authors (AV) from the Lorano Quarry, Carrara, Tuscany, Italy. Sample M0 was previously published as the untreated control by Voigtländer et al. (See Supporting Information of ref. [30]).

Here, sample M0 was analyzed during the December 2022 beamtime, and area 30 from this sample was presented.

3.1. Sample Preparation

All samples were cut with a low-speed diamond saw using Na_2CO_3 (22 g L^{-1}) as a coolant, then rinsed in ethanol, and embedded into EpoFix (EMS, Hatfield, PA, USA). They were then ground with increasingly fine SiC grit (320, 600, 800, 1200, 4000, Buehler, Lake Bluff, IL, USA), polished with 300 nm Al_2O_3 powder (MicroPolish Powder, Buehler, Lake Bluff, IL, USA) suspended in Na_2CO_3 (22 g L^{-1}), then with 50 nm Al_2O_3 (Master-Prep Suspension, Buehler, Lake Bluff, IL, USA), dialyzed against Na_2CO_3 (22 g L^{-1}) for 24 h.

All samples were then coated with 1 nm Pt in the area to be analyzed by PEEM, and with 40 nm around it. Both coatings were done with a Cressington 208HR sputter coater with a rotary tilt stage and a precision Cressington thickness controller MTM20 (both from Cressington Scientific Instruments, Watford, UK, sold by Ted Pella, Inc.), as described in detail before.[31,32]

3.2. Polarization-Dependent Imaging Contrast (PIC) Mapping

Polarization-dependent Imaging Contrast mapping or PIC mapping[33] is a method that uses PhotoEmission Electron Microscopy (PEEM) to image the sample surface[34,35], measure the *c*-axis orientation in 3D space, and display it in 2D images with quantitative color-coding. PIC mapping is based on X-ray linear dichroism at the O *K*-edge.[36] The resolution of PEEM images was 20–60 nm in this work, depending on magnification, the probing depth was 5 nm at the oxygen *K*-edge[32] and the *c*-axis orientation measured by PIC mapping resolution was ≈2°.[37] As mentioned in Table 1, the angle between *c*-axes measured by PIC mapping, termed γ, was different from δ because the smallest angle *c*-axes form in 3D space was chosen in PIC mapping, thus, if δ was >90° then $\gamma = 180° - \delta$.

PIC mapping data were acquired on PEEM-3 at the Advanced Light Source (ALS), Lawrence Berkeley National Laboratory (LBNL), which is a PhotoEmission Electron Microscope.[34,35,37,38] The spatial resolution varied between 45 and 56 nm, and was limited by the pixel sizes selected, not by the optics resolution, which is 20 nm at best.[33,35,38]

In each area, multiple PIC maps were collected, partly overlapping, and then stitched together in Adobe Photoshop 2023 for Mac, using the "Edit, Auto-Blend Layers" tool. Twin thicknesses were measured in Photoshop using the "Image, Analyze, Set Measurement Scale, Custom" tool, and exporting all measurements into Microsoft Excel 16.71 for Mac to obtain the statistical analysis in Table 3.

3.3. X-Ray Absorption Near-Edge Structure (XANES) Spectroscopy

One of the *Pm* shells and its prisms and twins was analyzed with X-ray absorption near edge structure (XANES) spectroscopy was using the same PEEM instrument used for PIC mapping. Ca *L*-edge spectra were acquired scanning the photon energy between 340–360 eV, with 0.1 eV steps, acquiring a PEEM image at each energy step, so, in the resulting stack of images each 56 nm pixel contains the full Ca spectrum. Ca spectra originated from the topmost 3 nm of the sample surface.[32,39] The two spectra in **Figure 3** were extracted from lines 100 pixel long, selected to be completely within the twin or the main crystal, and correspondingly labeled.

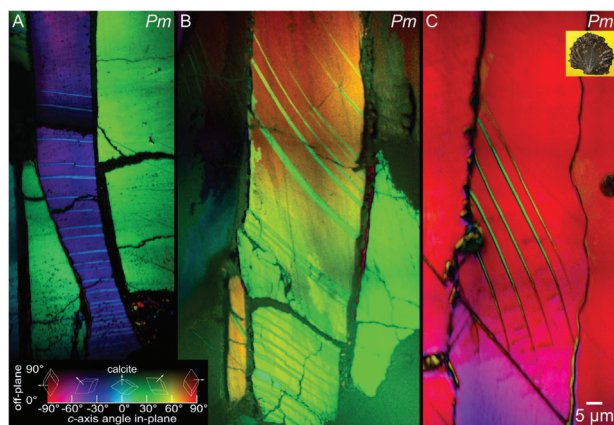### 3.4. Electron Back Scatter Diffraction (EBSD)

EBSD data were collected on a Zeiss EVO 10 scanning electron microscope, using an EDAX AMETEK DigiView EBSD detector. The first ever paper on the Kikuchi patterns that produce EBSD was published in 1954 by Alam, Pashley, and Nicholson.[40] Since then, much progress was made in instrumentation and sample preparation, resulting in many wonderful papers in materials science, biomineralization, and earth sciences.[41,42]

In this work, calcite twins were measured and assigned from the pole figures in **Figure 7**. The pole figures were generated using MATLAB with the MTEX toolbox for displaying crystallographic textures from EBSD data.

EBSD was the most quantitative and accurate method available to do these experiments and measure the twin type precisely. It is surface sensitive; therefore, it detected one crystal at a time not many crystals in depth as hard X-ray methods do, could analyze embedded and polished entire shells, with many prisms in their original position and configuration. Transmission electron microscopy (TEM) and electron diffraction would also be quantitative and informative, but only for individual twins, extracted from microscopic areas of the shell. TEM was not well-suited to analyze many twins at the micro-scale as done here with EBSD.

4. Results

We first observed calcite twinning in various locations of the calcite prismatic layers of three different Tahitian pearl oysters from *Pm*, as shown in the PIC maps of Figure 1. In a PIC map, color displays in 2D the 3D orientation of the calcite crystal *c*-axis, with hue and brightness corresponding to the in-plane and off-plane angle of the *c*-axis, respectively, as shown in the color bar of Figure 1 and described previously.[15,36,43] Each prism in *Pm* is not a single crystal, as previously observed.[44,45] It gradually changes in orientation; thus, it appears as a gradient of color in the PIC maps of Figure 1. Calcite twins are present in the three prisms of Figure 1: twins are distinct from the calcite prism, and they appear as parallel layers of a distinct, but consistent color. Parallel twins are not connected in space, but they are consistently colored because they have the same misorientation with respect to the calcite prism crystal. The thickness of the twins in *Pm*

ADVANCED
SCIENCE NEWS
www.advancedsciencenews.com

ADVANCED
FUNCTIONAL
MATERIALS
www.afm-journal.de

Figure 1. Polarization-dependent Imaging Contrast maps (PIC maps) of calcite prisms from the prismatic layers of three different *Pinctada margaritifera* (*Pm*) shells. A photo of a *Pm* shell, seen from the outside, where the calcite prisms are, is presented on top right. Twins are evident in all three panels, and they appear as layers of differently oriented and colored crystals. Notice that multiple twin layers are parallel to one another and similarly or identically colored. Calcite prisms in *Pm* are not single crystals of calcite. Most prisms gradually change in crystal orientation, displayed as a gradient of colors in PIC maps (blue to purple in A, green to red in B), and magenta to red in C)). Fascinatingly, as the calcite prism crystal tilts in orientation the twins curve in morphology. This is most evident in the central prisms in (B,C). The scale bar in (C) applies to (A–C).

Figure 1 varies between 0.2–3.1 μm, as summarized in Table 3, thus we observe both nanotwins and microtwins, as defined by Zhao et al.[46]

Interestingly, when the calcite prism crystal orientation gradually tilts, the shape of the microtwins curves in space. This is most
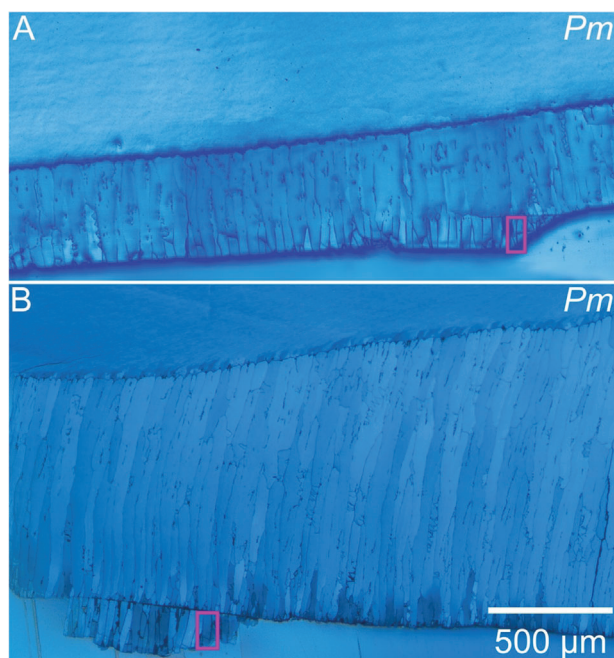
evident for the curving twins at the center and top of Figure 1B, or the twins at the bottom of Figure 1C. Correspondingly, the crystal around curved twins has a steep gradient of color, meaning that the prism crystal orientation changes gradually and rapidly.

The twins in Figure 1 were in prisms adjacent to fractured lamellae in *Pm*. Figure 2 documents this observation.

The twins are spectroscopically identical at the Ca *L*-edge to the main calcite crystal of the prism, as shown in Figure 3. Notice that the twins are completely invisible at the calcium *L*-edge (Figure 3B), as they are with other methods, such as scanning electron microscopy. They are, however, unequivocally composed of calcite, which is distinct from all other minerals at the Ca *L*-edge[36,47] especially in the peaks 2 and 4 energy regions, as labeled in Figure 3C.

We then explored other shells from the California red abalone *Haliotis rufescens* and found several twinned prisms, as displayed in **Figure 4**.

We analyzed another bivalve shell from *Ar* and found twins in *Ar* prisms as well. All calcite twins in *Ar* occurred near the outer surface of the shell in each prism, suggesting that the outer surface of the shell was twinned in response to mechanical stress. **Figure 5** shows this result in two regions of the same *Ar* shell cross-section. In all PIC maps in Figures 1, 4, and 5, the shell cross-sections are oriented similarly, with the outer shell surface at the bottom, well distinct from the embedding epoxy, which appears black in all PIC maps because it does not vary with X-ray polarization.
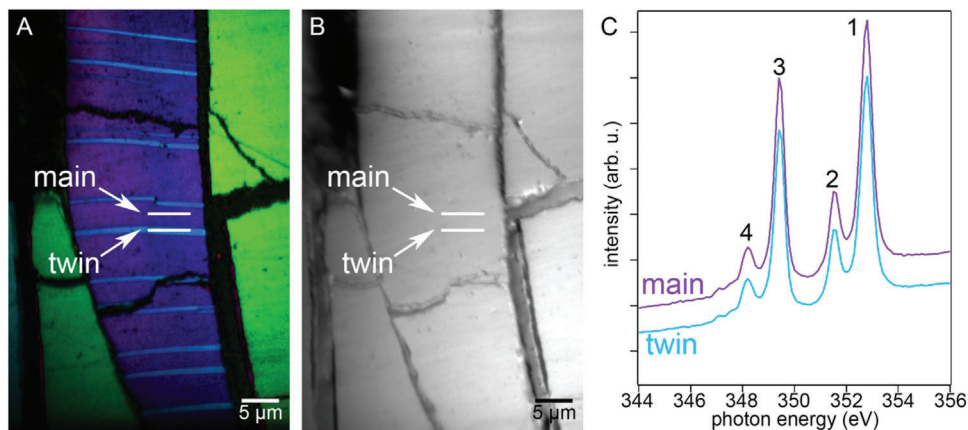
To test the hypothesis that the observed twins in mollusk shells are the result of mechanical stress, we indented some of the mollusk shells using a diamond scribe and imaged the resulting twins with optical microscopy. **Figure 6** shows the results of this qualitative test. Notice the twins that appeared after scratching the surface, but were absent before.

To validate both PIC mapping and observations in shells, we analyzed a Carrara marble sample known to have extensive twinning due to mechanical stimuli, such as compaction or shear deformation after metamorphism and recrystallization.[48] We found that indeed most calcite crystals in Carrara marble were twinned. This validates the PIC mapping method for detecting calcite twins.

Furthermore, we measured the precise orientation of twins with respect to the calcite prism crystal using EBSD, in three of the shells and one Carrara marble sample, in precisely the same locations as Figures 1, 4, and 5 (Figure 7).

Quantitative analysis of pole figures obtained from EBSD data revealed that all the twins observed in Carrara marble are e-twins ($01\bar{1}8$, with *c*-axes 127° apart), as shown in the pole figures in **Figure 8** and **Table 2**. E-twins have the lowest critical resolved shear stress at low temperatures and are commonly interpreted to be twins induced by purely mechanical stimuli.[49]

All twins observed in mollusk shells here are also e-twins, thus, the *c*-axes misorientation is $\delta = 127°$ or, choosing to measure the smallest angle between two axes, $\gamma = 180° - 127° = 53°$. The latter convention is typically used in PIC mapping (Table 1). All twins in mollusk shell prisms were indexed as calcite in EBSD, not as other mineral crystals, as already shown by Ca *L*-edge spectroscopy in Figure 3.

Figure 2. Polarized Light Micrograph (PLM) of *Pm* shells, indicating with magenta boxes the locations of twins in Figure 1A,B. The same scale bar applies to A,B).

ADVANCED
SCIENCE NEWS

www.advancedsciencenews.com

ADVANCED
FUNCTIONAL
MATERIALS

www.afm-journal.de

Figure 3. Ca spectroscopy in a *Pm* shell. A) The same PIC map as in Figure 1A, acquired at the O *L*-edge, showing two lines along which Ca *L*-edge spectra were acquired. B) Photoelectron image of the same region at the Ca *L*-edge, where the twins do not show any contrast. The two lines, identically positioned to those in (A), are 1 pixel high and 100 pixels long. Each pixel is 56 nm. C) X-ray absorption near edge structure (XANES) spectra, acquired at the Ca *L*-edge, show that the Ca spectra from the twin and the main crystals are identical, and that both are characteristic of calcite, having four sharp peaks labeled 1–4.
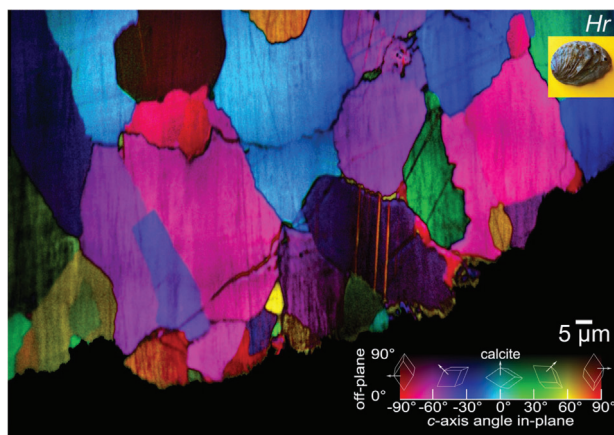
Table 2 shows the precise results for misorientation angle δ measured by EBSD for pairs of twins.

A summary of all twin thicknesses, measured from the PIC maps in Figures 1, 3, 4, 6 and others not shown, are presented in **Table 3**. Carrara marble has the most diverse twin thicknesses, varying from <0.2 µm to >15 µm, and correspondingly the greatest standard deviation. The mean thickness of twins in Carrara marble increases with temperature, as shown in lab experiments by Rybacki et al..[8]
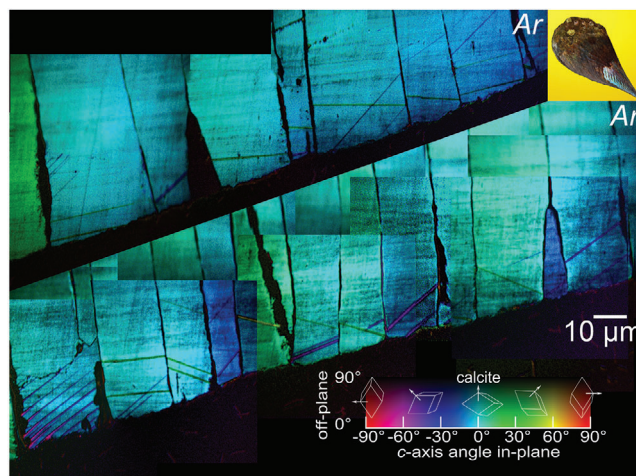
5. Discussion

### 5.1. First Observation of Twins in Mollusk Shell Calcite Prisms

We observed twins in the calcite prisms of three different mollusk shells, including two bivalves (*Pm* and *Ar*) and a gastro-

Figure 5. PIC map of the calcite twins within calcite prisms in two areas of an *Atrina rigida* (*Ar*) shell. A photo of an *Ar* shell outside is on top right. Notice the calcite twins consistently near the outside surface of the shell (bottom). The same scale bar applies to both areas.
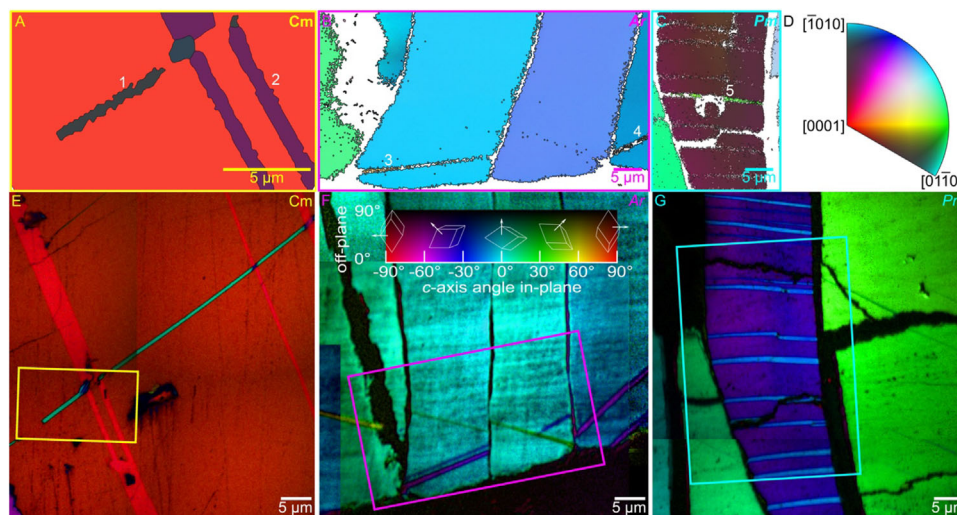

Figure 4. PIC map of the calcite twins in a *Haliotis rufescens* (*Hr*) shell. A photo of an *Hr* shell outer surface is on top right. In four of the calcite prisms, twins appear as differently colored, parallel lines. The location of these twins is near, but not exactly at the outer surface of the shell. The embedding epoxy appears black at the bottom of this PIC map.
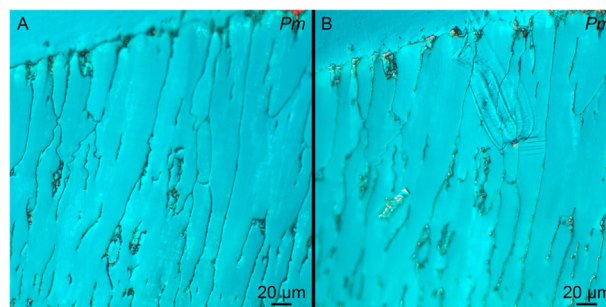
Figure 6. Visible light micrographs of *Pm* calcite prisms before A) and after B) scratching the surface with a diamond scribe. The aragonite nacre layer appears on top left of this polished cross-section, calcite prisms are everywhere else in the figure. Organic envelopes frequently separate calcite prisms. Comparing (A,B) it is evident that a single prism is completely untwinned before scratching and twinned after.

2304288 (5 of 9)

**ADVANCED
SCIENCE NEWS**

www.advancedsciencenews.com

**ADVANCED
FUNCTIONAL
MATERIALS**

www.afm-journal.de

Figure 7. A–C) Electron Back-Scatter Diffraction (EBSD) micrographs of a region of Carrara marble (Cm), *Atrina rigida* shell (*Ar*), and *Pinctada margaritifera* shell (*Pm*). All EBSD micrographs are Inverse Pole Figures (IPFs) that display in color the orientation of the crystal in each pixel. The EBSD-IPF color legend is in D). All EBSD-IPFs show extensive twins in calcite crystals, geologic and biogenic. E–G) PIC maps of the same regions, geologic and biogenic, where the boxes indicate the regions analyzed by EBSD. Where twins are thicker than ≈0.5 μm, EBSD captures them as well as PIC mapping, when they are thinner EBSD cannot capture them, as demonstrated by the green twins at the bottom of (F), which cannot be indexed by EBSD in (B). The twins labeled 1–5 in (A–C) could be indexed by EBSD and formed the angles with the calcite marble grain or prism crystal displayed in Table 2.

pod (*Hr*). Zhao et al. defined as nanotwins those observed to be 20–300 nm in thickness, and microtwins between 0.8 and 10 μm.[46] The twins we observed here in mollusk shell calcite prims were between 200 nm and 3 μm, we therefore chose to call them both nanotwins and microtwins.[46] For brevity, however, in all figures we just called them twins.

Intra-crystalline aragonite, but not calcite twins were previously observed to occur naturally in mollusk shells.[18,25] (Inter-crystalline formation twins were observed between calcite prisms in the ribs of *Pinna nobilis* shells, and those are formation twins.)[21] Calcite twins were induced artificially by nanoindentation in the foliated calcite of *Placuna placenta*.[7] The multiple parallel and intersecting twins within calcite prisms, described here, were not previously reported. We observed them consistently in multiple shells, and document their size, morphology, and precise orientation with nanoscale resolution.

5.2. Curved Twins

Twins are observed to curve in *Pm*, not in *Hr* and *Ar*. This is understandable, because *Pm* prisms are known not to be single crystals of calcite, but to have gradient orientations, in which the crystal lattice tilts gradually in space.[44,45] *Hr* and *Ar* prisms, instead are known to be single crystalline calcite and correspondingly the twins in them are morphologically straight, as expected, and previously observed in innumerable geologic studies and in Carrara marble in this work.

Curved twins in geologic samples are typically interpreted as evidence of two distinct phenomena: i) temperatures >200 °C and the onset of glide along r- and f-slip systems[6,49] or ii) lattice distortion of the calcite prism crystal, which can include complex sub-grain structure, heterogeneous dislocation densities, impurities, residual stress, etc..[9,50] It is unlikely that *Pinc-*

tada shells were ever exposed to 200 °C temperatures, thus, the latter interpretation is preferred here. In this case, the lattice distortion at the origin of curved twins is the gradient orientation observed in the calcite prisms of all six species of *Pinctada* recently analyzed.[45] As far as we know, curved twins have never been observed previously in mollusk shells or any other biomineral.
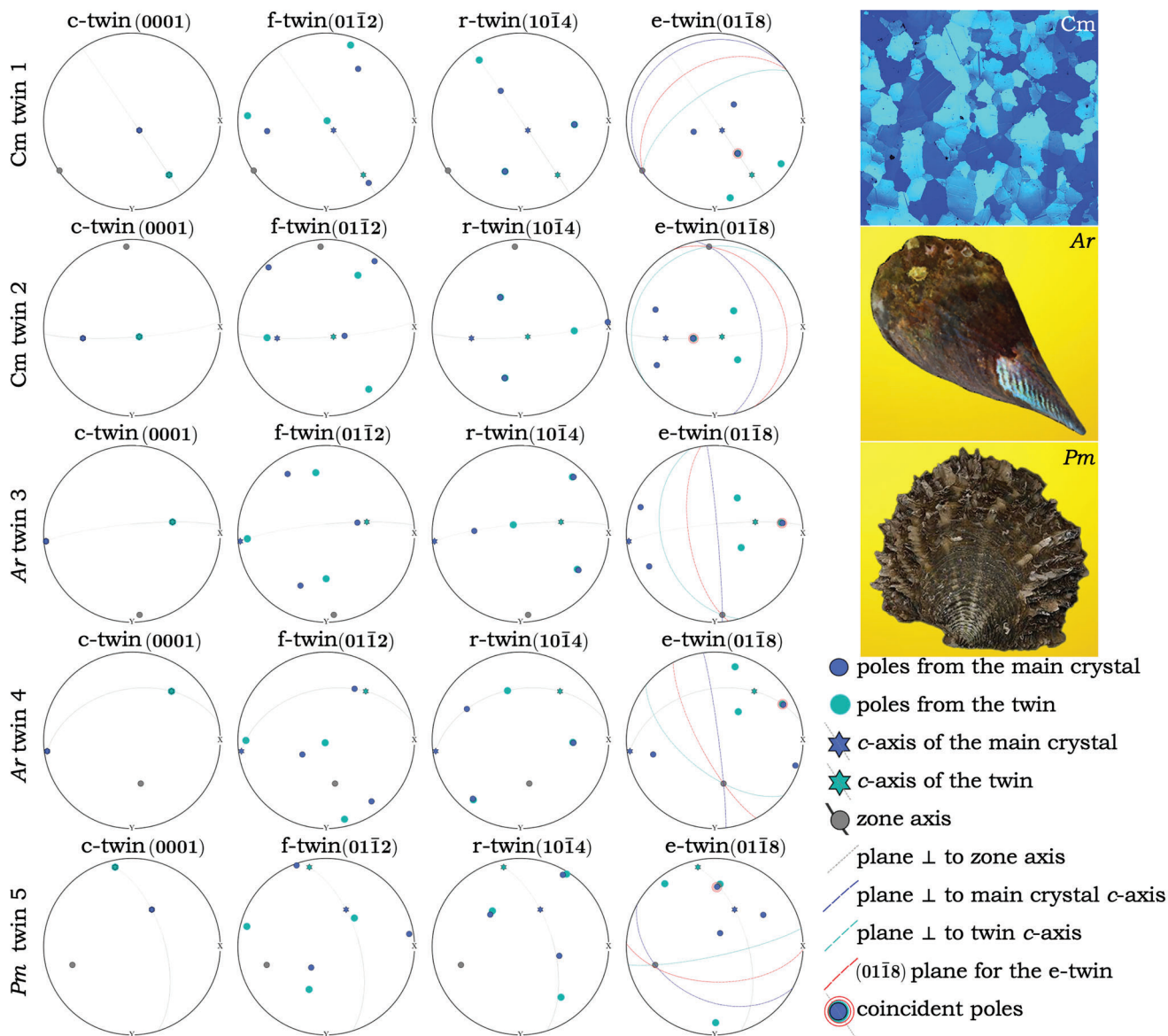
5.3. Location of Twins in Mollusk Shell Calcite Prisms Suggests Deformation Twinning

The *Pm* twins (Figure 1) were present in locations suggesting that damage occurs near the outer surface of the shell. We in fact observed twins only appearing in prisms adjacent to fractured lamellae (Figure 2) in *Pm*. Similarly, in *Ar* and *Hr* twinned prisms were located near the outer surface of the shell (Figures 4 and 5).

It remains unclear why twins observed in shells are more homogeneous in size, varying only between 0.2 to 3 μm, whereas twins in Carrara marble have a much greater spread of sizes from 0.2 to 15 μm. Thinner twins may be due either to lower mechanical stimuli in the biogenic case compared to the geologic, or to materials composition, for instance, the presence of proteins interspersed with calcite crystals in biogenic, but not geologic calcite. Alternatively, the lower temperatures to which mollusk shells are exposed, never exceeding ≈50 °C, even in tidal pools may only induce thinner twins, whereas the greater temperatures experienced by Carrara marble may result in thicker twins, as shown in lab experiments.[8]

The location of twins in all shells studied here, but especially in *Ar* (Figure 5), near the outer surface of the shell suggests damage-induced deformation rather than formation twinning. The most commonly observed deformation twinning is the e-type twinning in geologic calcite.[2,9] This is in fact the twin type

ADVANCED
SCIENCE NEWS
www.advancedsciencenews.com

ADVANCED
FUNCTIONAL
MATERIALS
www.afm-journal.de

Figure 8. Four pole figures for each of the five twins in Figure 7 in each row. Twins 1 and 2 are from Carrara marble (Cm), 3 and 4 from *Atrina rigida* (*Ar*) and twin 5 from *Pinctada margaritifera* (*Pm*). In each row, the four pole figures for the four common calcite twin laws (Table 1) indicate that all the twins analyzed here have a $(01\bar{1}8)$ twin plane, making them e-twins. Blue dots are poles from the main crystal (calcite grain in Cm, or prism in *Ar* and *Pm*), green dots are poles from the twin. *C*-axis poles are stars. The zone axis is the line where the two planes perpendicular to the *c*-axes of the two crystals intersect. The zone axis is perpendicular to both *c*-axes. The zone axes are grey dots in all panels, and the planes perpendicular to them are grey great circles. In all pole figures on the right, the coincident blue and green $(01\bar{1}8)$ poles are identified with a red double circle. In these pole figures, the blue and green great circles indicate the planes perpendicular to the *c*-axes of the two crystals, the red great circle is the $(01\bar{1}8)$ twin plane.

we observed in Carrara marble here and confirmed by many other observations.[2,9] Thus, the observation of e-twins corroborates our interpretation based on location in mollusk shell calcite prisms. These two results support one another and, combined, twin location and type, strongly suggest deformation twinning.

Figure 6 supports deformation twinning as well: it shows that twins in shell calcite prisms can result from mechanical damage.

Deformation twins may be beneficial to the living organism because they would localize damage as observed by Li and Ortiz in the calcite of a different shell and mesostructure, the lamellar

Table 2. Angles δ between *c*-axes of the calcite prism crystal and the twins labeled 1–5 in Figure 7. All five twins are e-twins.

	Angle δ from EBSD	Calcite twin type
Figure 7A twin 1	127.7°	e-twin $(01\bar{1}8)$
Figure 7A twin 2	127.2°	e-twin $(01\bar{1}8)$
Figure 7B twin 3	126.6°	e-twin $(01\bar{1}8)$
Figure 7B twin 4	126.0°	e-twin $(01\bar{1}8)$
Figure 7C twin 5	125.8°	e-twin $(01\bar{1}8)$

Table 3. Quantitative data on all twins in Figures 1, 4, 5, and 7. The table displays how many twins were observed in each figure, the minimum and maximum thickness measured, as well as the average and standard deviation. The thinnest twin in mollusk shells was 0.2 µm and the thickest 3.06 µm. On average, all twins were ≈0.5 to ≈1.0 µm, with a significant spread in each shell, ≈0.3–0.6 µm. Many more PIC maps were acquired on Carrara marble than displayed in Figure 7; all were counted in this table.

Sample	Pm	Pm	Pm	Hr	Ar	Cm
Figure	1A	1B	1C	4	5	7 and others
# twins measured	29	23	10	16	51	47
min twin thickness (µm)	0.20	0.56	0.78	0.43	0.28	0.17
max twin thickness (µm)	1.30	3.06	1.56	1.07	0.89	15.47
average twin thickness (µm)	0.60	1.02	1.25	0.74	0.54	1.25
St Dev twin thickness (µm)	0.28	0.59	0.24	0.17	0.13	2.41

microstructure of *Placuna placenta*,[7,20] where deformation twins arrest or deflect crack propagation[7] and toughen the biomineral. Tougher shells last longer and better protect the soft-bodied mollusk inside them; therefore, they may provide better sheltering and longevity to the forming animal. Li and Ortiz measured a factor of 10 toughening after artificial nanoindentation and calcite nanotwinning of *Placuna placenta* shells[7] and Shin et al. observed a significant contribution to toughening by aragonite nanotwinning in the crossed-lamellar structure of *Strombus gigas* shells.[25] Both effects were observed at the nano- or atomic-scale in calcite or aragonite nanotwins.

Here we observe microtwins and nanotwins in mollusk shells. The same crack-deflection mechanisms occurring at the nanoscale also occur at the microscale.[45] Furthermore, nano- or micro-scale toughening is well known to increase at larger scales, as elegantly demonstrated by the crack-deflecting layering of silica sponge spicules.[51] In general, toughness at the micro-scale is accompanied by even greater toughness at the macro-scale.[45] We did not measure toughness in the present study, because it was previously measured by other authors, before and after twinning, albeit in different shell mesostructures[18,24,25,27,29] or in geologic calcite.[4,9,42,48-50,52] Thus, we cannot assign a function to the twins observed here. In a completely different material, cryoforged titanium, Zhao et al. showed that nanotwins and microtwins confer strength and ductility to the material at the macroscopic scale.[46] Zeng et al. showed that twinning confers toughness to nanotwinned copper.[53] Twins in cryoforged titanium and in mollusk shell calcite are remarkably similar in morphology, size, and orientation. This similarity does not demonstrate a function for nanotwinning in calcite shell prisms. It only suggests a potential function.

6. Conclusion

As far as we know this was the first observation of naturally occurring twinning within mollusk shell calcite prisms. Furthermore, we observed damage localizing calcite twins near the outer surface of shells, and unprecedented curving twins. All twins thus far observed were e-twins, but in principle any other twin type is possible in prisms. Further studies will determine how widespread twinning is in calcite prisms across species, what type

of twins will be observed, and if the intracrystalline organics play any role in twinning. The future of calcite twins is crystal clear.

Conflict of Interest

The authors declare no conflict of interest.

Data Availability Statement

The data that support the findings of this study are available from the corresponding author upon reasonable request.

[1] W. L. Bragg, *Proc. R. Soc. London, Ser. A* **1924**, *105*, 16.
[2] R. P. Richards, *Rocks Miner.* **1999**, *74*, 308.
[3] B. Pokroy, M. Kapon, F. Marin, N. Adir, E. Zolotoyabko, *Proc. Natl. Acad. Sci. U. S. A.* **2007**, *104*, 7337.
[4] D. Barber, H.-R. Wenk, *Phys. Chem. Miner.* **1979**, *5*, 141.
[5] A. Côté, R. Darkins, D. Duffy, *Phys. Chem. Chem. Phys.* **2015**, *17*, 20178.
[6] D. A. Ferrill, A. P. Morris, M. A. Evans, M. Burkhard, R. H. Groshong, C. M. Onasch, *J. Struct. Geol.* **2004**, *26*, 1521.
[7] L. Li, C. Ortiz, *Nat. Mater.* **2014**, *13*, 501.
[8] E. Rybacki, B. Evans, C. Janssen, R. Wirth, G. Dresen, *Tectonophysics* **2013**, *601*, 20.
[9] M. Burkhard, *J. Struct. Geol.* **1993**, *15*, 351.
[10] M. Friedman, F. Conger, *J. Geol.* **1964**, *72*, 361.
[11] Z. Deng, Z. Jia, L. Li, *Adv. Sci.* **2022**, *9*, 2103524.
[12] A. G. Checa, D. Gaspard, A. González-Segura, J. N. Ramírez-Rico, *Cryst. Growth Des.* **2009**, *9*, 2464.
[13] J. Lastam, E. Griesshaber, X. Yin, U. Rupp, I. Sánchez-Almazo, M. Heß, P. Walther, A. Checa, W. Schmahl, *Sci. Rep.* **2023**, *13*, 2189.
[14] P. L. O'Neill, *Science* **1981**, *213*, 646.

**ADVANCED
SCIENCE NEWS**

www.advancedsciencenews.com

**ADVANCED
FUNCTIONAL
MATERIALS**

www.afm-journal.de

[15] P. U. P. A. Gilbert, *MRS Bull.* **2023**, *48*, 413.

[16] J. D. Taylor, *Bull. Br. Mus. (Nat. Hist.), Zool.* **1969**, *3*, 1.

[17] F. Barthelat, H. Espinosa, *Exp. Mech.* **2007**, *47*, 311.

[18] S. Kamat, X. Su, R. Ballarini, A. Heuer, *Nature* **2000**, *405*, 1036.

[19] A. G. Checa, F. J. Esteban-Delgado, A. B. Rodríguez-Navarro, *J. Struct. Biol.* **2007**, *157*, 393.

[20] L. Li, C. Ortiz, *Adv. Mater.* **2013**, *25*, 2344.

[21] K. Nalepka, K. Berent, A. G. Checa, T. Machniewicz, A. J. Harris, P. Nalepka, M. Strąg, Ł. Maj, A. Szkudlarek, M. Bieda, *Mater. Sci. Eng. A* **2022**, *829*, 142163.

[22] M. E. Kunitake, L. M. Mangano, J. M. Peloquin, S. P. Baker, L. A. Estroff, *Acta Biomater.* **2013**, *9*, 5353.

[23] H. Mukai, K. Saruwatari, H. Nagasawa, T. Kogure, *J. Cryst. Growth* **2010**, *312*, 3014.

[24] H. Mutvei, *Zool. Scr.* **1978**, *7*, 287.

[25] Y. A. Shin, S. Yin, X. Li, S. Lee, S. Moon, J. Jeong, M. Kwon, S. J. Yoo, Y.-M. Kim, T. Zhang, *Nat. Commun.* **2016**, *7*, 10772.

[26] K. Faber, A. G. Evans, *J. Am. Ceram. Soc.* **1983**, *66*, 94.

[27] R. O. Ritchie, *Philos. Trans. R. Soc., A* **2021**, *379*, 20200437.

[28] a) E. Munch, M. E. Launey, D. H. Alsem, E. Saiz, A. P. Tomsia, R. O. Ritchie, *Science* **2008**, *322*, 1516; b) U. G. Wegst, H. Bai, E. Saiz, A. P. Tomsia, R. O. Ritchie, *Nat. Mater.* **2015**, *14*, 23; c) B. Pokroy, A. Fitch, E. Zolotoyabko, *Adv. Mater.* **2006**, *18*, 2363.

[29] a) F. Barthelat, *Bioinspiration Biomimetics* **2010**, *5*, 035001; b) Z. Deng, L. Li, *ACS Biomater. Sci. Eng.* **2023**, *9*, 3900.

[30] A. Voigtländer, K. Leith, M. Krautblatter, *J. Geophys. Res.: Solid Earth* **2018**, *123*, 3780.

[31] G. De Stasio, B. H. Frazer, B. Gilbert, K. L. Richter, J. W. Valley, *Ultramicroscopy* **2003**, *98*, 57.

[32] P. U. P. A. Gilbert, in *Biomineralization Sourcebook, Characterization of Biominerals and Biomimetic Materials* (Eds.: E. DiMasi, L. B. Gower), CRC Press, Boca Raton, FL **2014**, 135.

[33] P. U. P. A. Gilbert, A. Young, S. N. Coppersmith, *Proc. Natl. Acad. Sci. U. S. A.* **2011**, *108*, 11350.

[34] G. De Stasio, M. Capozi, G. F. Lorusso, P. A. Baudat, T. C. Droubay, P. Perfetti, G. Margaritondo, B. P. Tonner, *Rev. Sci. Instrum.* **1998**, *69*, 2062.

[35] G. De Stasio, L. Perfetti, B. Gilbert, O. Fauchoux, M. Capozi, P. Perfetti, G. Margaritondo, B. P. Tonner, *Rev. Sci. Instrum.* **1999**, *70*, 1740.

[36] R. T. DeVol, R. A. Metzler, L. Kabalah-Amitai, B. Pokroy, Y. Politi, A. Gal, L. Addadi, S. Weiner, A. Fernandez-Martinez, R. Demichelis, J. D. Gale, J. Ihli, F. C. Meldrum, A. Z. Blonsky, C. E. Killian, C. B. Salling, A. T. Young, M. A. Marcus, A. Scholl, A. Doran, C. Jenkins, H. A. Bechtel, P. U. P. A. Gilbert, *J. Phys. Chem. B* **2014**, *118*, 8449.

[37] I. C. Olson, A. Z. Blonsky, N. Tamura, M. Kunz, B. Pokroy, C. P. Romao, M. A. White, P. U. Gilbert, *J. Struct. Biol.* **2013**, *184*, 454.

[38] J. Feng, A. Scholl, in *Science of Microscopy*, Springer, New York, NY **2007**, 657.

[39] B. H. Frazer, B. Gilbert, B. R. Sonderegger, G. De Stasio, *Surf. Sci.* **2003**, *537*, 161.

[40] M. Alam, M. Blackman, D. W. Pashley, *Proc. R. Soc. London, Ser. A* **1954**, *221*, 224.

[41] a) A. J. Wilkinson, T. B. Britton, *Mater. Today* **2012**, *15*, 366; b) A. Pérez-Huerta, Y. Dauphin, J. P. Cuif, M. Cusack, *Micron* **2011**, *42*, 246; c) M. Cusack, Y. Dauphin, P. Chung, A. Pérez-Huerta, J.-P. Cuif, *J. Struct. Biol.* **2008**, *164*, 96; d) E. Griesshaber, W. W. Schmahl, R. Neuser, T. Pettke, M. Blüm, J. R. Mutterlose, U. Brand, *Am. Mineral.* **2007**, *92*, 722; e) L. Burlini, K. Kunze, *Phys. Chem. Earth (1956–1998)* **2000**, *25*, 133; f) A. Barnhoorn, M. Bystricky, L. Burlini, K. Kunze, *J. Struct. Geol.* **2004**, *26*, 885.

[42] M. Pieri, L. Burlini, K. Kunze, I. Stretton, D. L. Olgaard, *J. Struct. Geol.* **2001**, *23*, 1393.

[43] a) B. Pokroy, L. Kabalah-Amitai, I. Polishchuk, R. T. DeVol, A. Z. Blonsky, C.-Y. Sun, M. A. Marcus, A. Scholl, P. U. P. A. Gilbert, *Chem. Mater.* **2015**, *27*, 6516; b) P. U. P. A. Gilbert, K. D. Bergmann, C. E. Myers, M. A. Marcus, R. T. DeVol, C.-Y. Sun, A. Z. Blonsky, E. Tamre, J. Zhao, E. A. Karan, N. Tamura, S. Lemer, A. J. Giuffre, G. Giribet, J. M. Eiler, A. H. Knoll, *Earth Planet. Sci. Lett.* **2017**, *460*, 281.

[44] a) A. G. Checa, J. T. Bonarski, M. G. Willinger, M. Faryna, K. Berent, B. Kania, A. González-Segura, C. M. Pina, J. Pospiech, A. Morawiec, *J. R. Soc., Interface* **2013**, *10*, 20130425; b) I. C. Olson, R. A. Metzler, N. Tamura, M. Kunz, C. E. Killian, P. U. P. A. Gilbert, *J. Struct. Biol.* **2013**, *183*, 180; c) V. Schoeppler, D. Stier, R. J. Best, C. Song, J. Turner, B. H. Savitzky, C. Ophus, M. A. Marcus, S. Zhao, K. Bustillo, *Adv. Mater.* **2021**, *33*, 2101358.

[45] A. J. Lew, C. A. Stifler, A. Tits, C. A. Schmidt, A. Scholl, A. Cantamessa, L. Müller, Y. Delaunois, P. Compère, D. Ruffoni, M. J. Buehler, P. U. P. A. Gilbert, *Adv. Mater.* **2023**, *35*, 2300373.

[46] S. Zhao, R. Zhang, Q. Yu, J. Ell, R. O. Ritchie, A. M. Minor, *Science* **2021**, *373*, 1363.

[47] a) Y. U. T. Gong, C. E. Killian, I. C. Olson, N. P. Appathurai, A. L. Amasino, M. C. Martin, L. J. Holt, F. H. Wilt, P. U. P. A. Gilbert, *Proc. Natl. Acad. Sci. U. S. A.* **2012**, *109*, 6088; b) Z. Zou, W. J. E. M. Habraken, G. Matveeva, A. C. S. Jensen, L. Bertinetti, M. A. Hood, C.-Y. Sun, P. U. P. A. Gilbert, I. Polishchuk, B. Pokroy, J. Mahamid, Y. Politi, S. Weiner, P. Werner, S. Bette, R. Dinnerbier, U. Kolb, E. Zolotoyabko, P. Fratzl, *Science* **2019**, *393*, 396.

[48] G. Molli, P. Conti, G. Giorgetti, M. Meccheri, N. Oesterling, *J. Struct. Geol.* **2000**, *22*, 1809.

[49] H.-R. Wenk, in *Preferred Orientation in Deformed Metals and Rocks: An Introduction to Modern Texture Analysis*, Academic Press, Inc, Orlando, FL **1985**, pp. 361–384.

[50] F. J. Turner, M. Orozco, *Contrib. Mineral. Petrol.* **1976**, *57*, 83.

[51] A. Miserez, J. C. Weaver, P. J. Thurner, J. Aizenberg, Y. Dauphin, P. Fratzl, D. E. Morse, F. W. Zok, *Adv. Funct. Mater.* **2008**, *18*, 1241.

[52] J. T. Fredrich, B. Evans, T. F. Wong, *J. Geophys. Res.: Solid Earth* **1989**, *94*, 4129.

[53] Z. Zeng, X. Li, X. Lu, T. Zhu, *Acta Mater.* **2015**, *98*, 313.